DALTON
FULL PAPER

Cyclooctatetraene ditungsten alkoxides: $W_2(\mu\text{-}\eta^5,\eta^5\text{-COT})(OR)_4$, where R = $CH_2{}^tBu$, ^iPr, and ^tBu

Bruce E. Bursten,* Malcolm H. Chisholm,* Michael L. Drummond, Judith C. Gallucci and Carl B. Hollandsworth

Department of Chemistry, The Ohio State University, Columbus, OH, USA.
E-mail: chisholm@chemistry.ohio-state.edu; bursten@chemistry.ohio-state.edu

Received 27th May 2002, Accepted 11th September 2002
First published as an Advance Article on the web 17th October 2002

Four equivalents of neopentanol, isopropanol, or t-butanol react with the cyclooctatetraene-bridged dimethylamide, $W_2(\mu\text{-}\eta^5,\eta^5\text{-COT})(NMe_2)_4$, to give the corresponding tetraalkoxides, $W_2(\mu\text{-}\eta^5,\eta^5\text{-COT})(OR)_4$, in greater than 70% yields. The alkoxide $W_2(COT)(OCH_2{}^tBu)_4$ can be made alternatively by reacting $W_2(COT)(O^tBu)_4$ with 4 equivalents of neopentanol. X-ray diffraction data for the t-butoxide compound indicate a $\mu\text{-}\eta^5,\eta^5$-COT ligand spans a W–W bond of distance 2.3887(1) Å. The t-butoxide is very similar in most structural parameters to the known $W_2(COT)(NMe_2)_4$ precursor as well as the bis-allyl compound $W_2(allyl)_2(NMe_2)_4$. The COT ring is fluxional about the metal–metal fragment, undergoing rapid 1,2-shifts on the NMR timescale as determined by ^1H EXSY NMR. The purple alkoxides exhibit maximum absorptions around 580 nm ($\varepsilon \sim 1700\ M^{-1}\ cm^{-1}$) in the visible region of the electronic absorption spectrum. This transition agrees well with DFT calculations on the model compound $W_2(\mu\text{-}\eta^5,\eta^5\text{-COT})(OH)_4$ that reveal the calculated HOMO–LUMO gap to be a 1.94 eV transition involving principally the metal d orbitals. The calculations also reveal the structure with an antifacial (η^5,η^5)-COT to be 13.7 kcal mol^{-1} more stable than the corresponding synfacial (η^4,η^4)-COT structure. In related studies, COT did not form adducts with $W_2(OCH_2{}^tBu)_6(py)_2$, $W_2(O^tBu)_6$, or $W_2(OCH_2{}^tBu)_8$ even upon heating to 80 °C for several hours.

Introduction

Ditungsten hexaalkoxides have proven to be a reactive template for the coordination and activation of a wide variety of unsaturated organic molecules such as alkynes, ethene, allenes, nitriles, aldehydes, ketones, and 1,3-dienes.[1a,b] Structural studies of 1,3-butadiene and isoprene adducts revealed an unusual mode of coordination wherein one carbon bridged the dimetal center and the remaining C_3 moiety was bonded to just one W in a manner resembling a π-allyl fragment.[2] Solution NMR studies confirmed this mode of binding and also indicated that the substrate binding was reversible. In a formal sense, the uptake of the 1,3-diene at the $(W{\equiv}W)^{6+}$ center represented an oxidation of the metals and a reduction of the diene: $W_2{}^{8+}(\mu\text{-}\eta^1,\eta^4\text{-}C_4H_6)(OR)_6$. Along those lines we felt that 1,3,5,7-cyclooctatetraene (COT) would quite probably bind to $W_2(OR)_6$ compounds, with an interesting mode of coordination.

Cotton and coworkers have investigated the structure and dynamic NMR behavior of a number of dinuclear, COT organometallics. Prime examples are $Fe_2(Me_4COT)(CO)_5$,[3] $Ru_2(COT)(CO)_6$,[4] $W_2(\eta^4\text{-COT})_2(\mu\text{-}\eta^5,\eta^5\text{-COT})$,[5,6] and $Mo_2(\eta^4\text{-COT})_2(\mu\text{-}\eta^5,\eta^5\text{-COT})$.[6] The synthesis of $Fe_2(\mu\text{-COT})(CO)_6$ has also been reported, as have detailed electronic structure calculations on several MM'(COT)Cp_2 and M(CrCp)(μ-COT)$(CO)_3$ compounds.[7a–d] It was these considerations, along with our recent preparation of $W_2(\mu\text{-}\eta^5,\eta^5\text{-COT})(NMe_3)_4$, that prompted the work we describe herein.[8a]

Results and discussion

Reactions of COT with ditungsten alkoxides

COT was added to hydrocarbon solutions of several known ditungsten alkoxides with no apparent reaction. As deduced by ^1H NMR spectroscopy, which showed only signals for free COT and the alkoxide starting material. Heating the solutions to 80 °C for several hours failed to initiate a reaction, even in the presence of greater than 100-fold excess of COT. At that temperature, eventual thermal decomposition of the alkoxide is deduced by ^1H NMR spectroscopy. Attempts to react the neopentoxide in the presence of a 10-fold excess of ethanol also failed to yield a product containing a bound COT ligand. According to mass spectrometry data, this reaction likely leads to the formation of a polynuclear alkoxide. The product(s) were soluble in toluene and other hydrocarbon solvents, but ^1H NMR spectroscopy indicated the absence of coordinated COT. It is anticipated that COT, unlike butadiene and isoprene, is too large a ligand to coordinate to the hexaalkoxides.

$W_2(\mu\text{-}\eta^5,\eta^5\text{-COT})(OR)_4$ compounds. Preparations, properties, and structures

Alcoholysis of $W_2(\mu\text{-}\eta^5,\eta^5\text{-COT})(NMe_2)_4$ with four equivalents of neopentanol, isopropanol, or t-butanol leads to the respective $W_2(\mu\text{-}\eta^5,\eta^5\text{-COT})(OR)_4$ compound. The reactions proceed with greater than 70% yields according to eqn. (1) and are accompanied by a striking color change from forest green to indigo. Alternatively, **1b** is made quantitatively upon addition of 4 equivalents of neopentyl alcohol to **1c** according to eqn. (2).

$$W_2(COT)(NMe_2)_4 + 4ROH \xrightarrow{\text{toluene}} W_2(COT)(OR)_4 + 4HNMe_2 \quad (1)$$

1 — **1a** R = $CH_2{}^tBu$; **1b** R = ^iPr; **1c** R = ^tBu

$$W_2(COT)(O^tBu)_4 + 4\ {}^tBuCH_2OH \longrightarrow W_2(COT)(OCH_2{}^tBu)_4 + 4\ HNMe_2 \quad (2)$$

The products are air-sensitive and soluble in aliphatic and aromatic hydrocarbons. The t-butoxide compound appears to be heat sensitive, decomposing under vacuum to make a green solid at temperatures above 50 °C. Attempts to obtain crystalline samples suitable for a single crystal X-ray diffraction were only successful for the t-butoxide. Only microcrystalline samples have been obtained for the neopentoxide and isopropoxide. However, the ^{1}H and ^{13}C NMR solution spectra are informative with respect to the molecular structure of the alkoxides.

At room temperature the COT ^{1}H resonances are not well resolved because the bridging COT is fluxional. At −30 °C and below in toluene-d_8 there are three well resolved multiplets in the integral ratio 2 : 4 : 2. This ratio is consistent with a ground-state structure having C_{2v} symmetry. In the case of the neopentoxide complex there is a single ^{t}Bu ^{1}H signal and an AX pair of doublets for the diastereotopic methylene protons. For the isopropoxide complex there is a septet for the methine protons and a pair of doublets arising from the diastereotopic methyl groups. The tertiary butoxide compound shows only the three sets of COT multiplets and a single ^{t}Bu resonance. Upon raising the temperature the signals associated with the bridging COT coalesce. VT EXSY data have shown that the exchange involves a 1,2-shift. That is H_a and H_b exchange with H_c but not with each other in the slow exchange regime (see Fig. 1). The assignment of the ^{1}H signals to H_a and H_b is ambiguous because each signal is of intensity two whereas the assignment of H_c is straightforward.

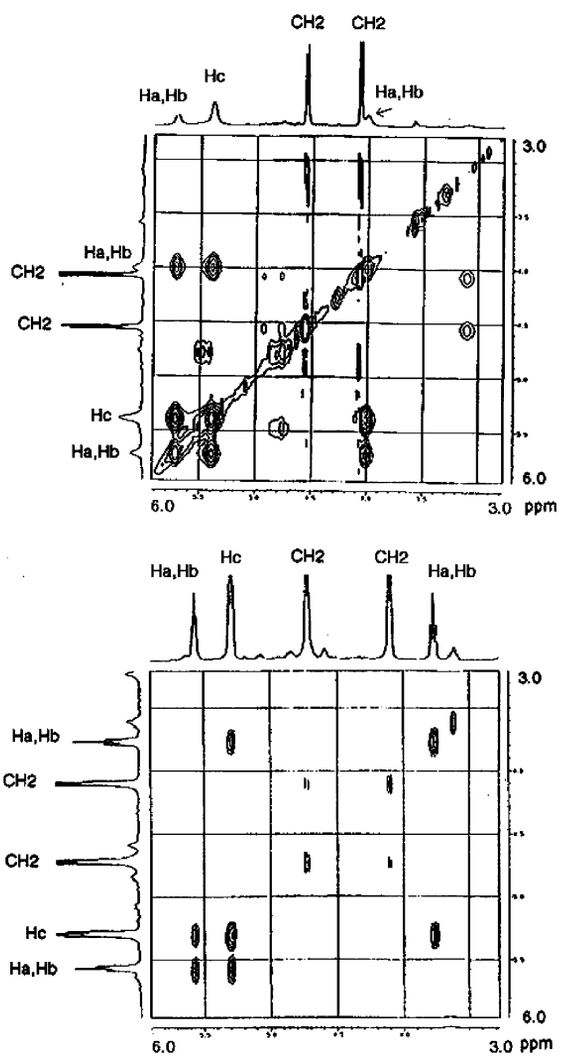

Fig. 1 400 MHz ^{1}H NMR EXSY spectrum showing chemical exchange between H_a, H_b, and H_c at room temperature (top spectrum) and diminished exchange between H_a and H_b at −50 °C (bottom spectrum).

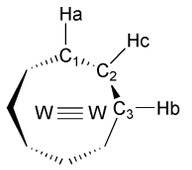

The NMR data are supported by the solid state structure of the t-butoxide compound (Fig. 2 and 3 and Tables 1 and 2). Ignoring the orientation of the O–t-butyl substituents, it is evident that the molecule possesses pseudo-C_{2v} symmetry with the COT ring bound in a μ-η^5,η^5 fashion. The W–W distance of 2.3887 (1) Å corresponds to a typical W–W triple bond length.[9] Assuming that the ring is formally a COT^{2-} ligand, the W–W fragment will be (W–W)$^{6+}$. This structure can be compared to a

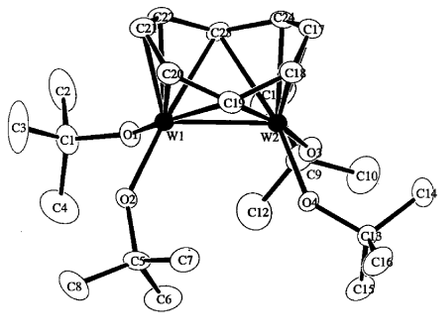

Fig. 2 View of **1c** showing the puckered nature of the COT ring (hydrogen atoms are omitted for clarity).

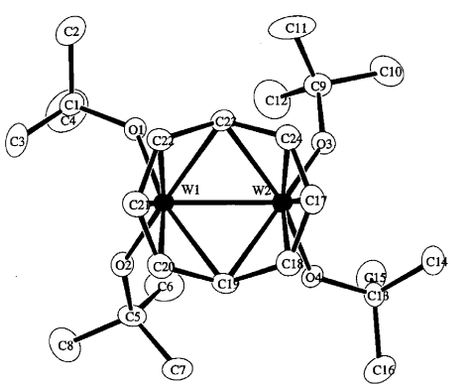

Fig. 3 View of **1c** looking down the virtual C_2 axis of symmetry (hydrogen atoms are omitted for clarity).

Table 1 Crystal data for $W_2(COT)(O^{t}Bu)_4$ (**1c**)

Empirical formula	$C_{24}H_{44}O_4W_2$
Formula weight	764.29
Temperature/K	150(2)
Wavelength/Å	0.71073
Crystal system	monoclinic
Space group	$P2_1/c$
a/Å	8.6049(1)
b/Å	12.7625(1)
c/Å	24.3617(2)
β/°	91.730(1)
Volume/Å^3	2674.18(4)
Z	4
$D_{calc.}$/Mg m^{-3}	1.898
μ/mm^{-1}	8.621
Reflections collected	55574
Independent reflections, R_{int}	6126, 0.035
Final R_1 [$I > 2\sigma(I)$][a]	0.0157
Final wR_2 [$I > 2\sigma(I)$][b]	0.0356
R_1 (all data)	0.0185
wR_2 (all data)	0.0364

[a] $F_{R_1} = \Sigma \| |F_o| - |F_c| \| / \Sigma |F_o|$. [b] $wR_2 = [\Sigma w (F_o^2 - F_c^2)^2 / \Sigma w (F_o^2)^2]^{1/2}$.

Table 2 Selected bond distances and angles for $W_2(COT)(O^tBu)_4$ (**1c**)

Bond lengths/Å		Bond angles/°	
W(1)–W(2)	2.3887(1)	O(1)–W(1)–O(2)	92.26(7)
W(1)–O(1)	1.934(2)	O(3)–W(2)–O(4)	90.22(7)
W(1)–O(2)	1.909(2)	O(1)–W(1)–W(2)	107.21(5)
W(2)–O(3)	1.916(2)	O(2)–W(1)–W(2)	115.45(5)
W(2)–O(4)	1.938(2)	O(3)–W(2)–W(1)	115.81(5)
W(1)–C(19)	2.453(2)	O(4)–W(2)–W(1)	108.65(5)
W(1)–C(20)	2.237(2)	O(1)–W(1)–(C19)	166.86(8)
W(1)–C(21)	2.324(3)	O(2)–W(1)–(C23)	174.82(8)
W(1)–C(22)	2.254(3)	O(3)–W(2)–C(19)	173.76(8)
W(1)–C(23)	2.413(2)	O(4)–W(2)–C(23)	168.13(8)
W(2)–C(17)	2.318(2)	C(1)–O(1)–W(1)	134.7(2)
W(2)–C(18)	2.244(2)	C(5)–O(2)–W(1)	145.9(2)
W(2)–C(19)	2.420(2)	C(9)–O(3)–W(2)	148.4(2)
W(2)–C(23)	2.440(2)	C(13)–O(4)–W(2)	135.08(14)
W(2)–C(24)	2.229(3)	C(17)–C(18)–C(19)	130.3(2)
C(17)–C(18)	1.409(4)	C(18)–C(19)–C(20)	127.2(2)
C(18)–C(19)	1.451(4)	C(19)–C(20)–C(21)	129.6(2)
C(19)–C(20)	1.448(4)	C(20)–C(21)–C(22)	127.6(2)
C(20)–C(21)	1.410(4)	C(21)–C(22)–C(23)	129.8(2)
C(21)–C(22)	1.424(4)	C(22)–C(23)–C(24)	127.5(2)
C(22)–C(23)	1.435(4)	C(17)–C(24)–C(23)	129.2(2)
C(23)–C(24)	1.447(4)	C(18)–C(17)–C(24)	127.7(2)
C(17)–C(24)	1.412(4)		

d^3–d^3 system with six eclipsed alkoxides, where two alkoxide ligands have been replaced with a COT ring. This analogy is explored further in the following section.

Computational results and bonding considerations

The bonding in $W_2(COT)(NH_2)_4$ has been examined previously using a fragment approach and the Fenske-Hall Molecular Orbital method.[8a] These studies provided a nice analysis of the major orbital interactions between the COT ring and the W_2 fragment, but did not allow for the calculation of total-energy properties, such as geometries and rotational barriers. Here we will present an analysis of the bonding and electronic structure of the model complex $W_2(COT)(OH)_4$, derived from relativistic density functional theory (DFT) calculations. The DFT method provides reliable total energies, which will allow us to predict geometric and energetic properties of the molecule.[10]

We will begin with a slightly different analysis of the COT–W_2 orbital interactions than was presented previously. In order to elucidate the major interactions between the COT ring and the $W_2(OH)_4$ fragment, we will start from a consideration of the metal–metal bonding in the well-known triply-bonded $W_2(OR)_6$ systems.[9] Although $W_2(OR)_6$ molecules are normally found in a staggered D_{3d} geometry, we will find it useful to examine the molecule in an eclipsed D_{3h} geometry. As we have pointed out previously, the six OR ligands in this complex serve to "remove" the W_2 δ and δ* MOs, which are formed from the W $5d_{x^2-y^2}$ and $5d_{xy}$ AOs, and the W 6s AOs from the metal–metal bonding manifold.[11] The remaining W 5d orbitals form the familiar set of metal–metal bonding and antibonding MOs, with the energetic order $\sigma (a_1') < \pi (e') < \sigma^* (a_2'') < \pi^* (e'')$ and a $\sigma^2\pi^4$ triple-bond electron configuration [Fig. 4a]. We will now remove two of the OH^- ligands to form a C_{2v} $[W_2(OH)_4]^{2+}$ fragment. This fragment retains the W–W triple bond, but the removal of two ligands significantly lowers the energy of four empty acceptor orbitals, two of which were W–O σ* (a_1 and b_1) and two of which were W–O π* (a_2 + b_2). Of these four acceptor orbitals, only two, the a_1 and the a_2, have the symmetry required to interact with the expected π_4 and π_5 COT^{2-} donor orbitals [Fig. 4d]. As such, the empty $15a_1$ (predominatly W–W δ) and the empty $9a_2$ (predominantly W–W π*) are primarily responsible for binding the COT^{2-} ligand.

Per usual, we will consider the ring to be the closed-shell COT^{2-} dianion. Under C_{2v} symmetry, the ordering of the π MOs of COT^{2-} is π_1 ($6a_1$) < π_2, π_3 ($5b_1$ and $5b_2$) < π_4, π_5 ($7a_1$ and $4a_2$) < π_6, π_7 ($6b_1$ and $6b_2$) < π_8 ($9a_1$), with π_1–π_5 filled [Fig. 4d]. The puckering of the ring that is observed in the complex lifts the degeneracy of the π MOs [Fig. 4e], but preserves this basic order. As mentioned above, the principal bonding interactions are expected to involve donation from the filled $7a_1$ and $4a_2$ MOs of COT^{2-} into the vacant acceptor orbitals on the $[W_2(OH)_4]^{2+}$ fragment. These interactions are shown in Fig. 4c. They are also apparent in Table 3, which lists the relevant W_2- and COT-based MOs of $W_2(COT)(OH)_4$. The interaction of the HOMO $4a_2$ of COT^{2-} with the $9a_2$ acceptor orbital of $[W_2(OH)_4]^{2+}$ leads to the filled $12a_2$ and empty $13a_2$ MOs of $W_2(COT)(OH)_4$ (Fig. 4c, dashed line). The donation from the $7a_1$ COT^{2-} MO to the $15a_1$ acceptor MO is complicated by the presence of a filled $13a_1$ $[W_2(OH)_4]^{2+}$ MO at nearly the same energy as the donor $7a_1$ COT^{2-} MO. The resulting filled–filled interaction leads to a slight elevation of the resulting $20a_1$ $W_2(COT)(OH)_4$ orbital (Fig. 4c, solid line). Other significant interactions between the COT^{2-} and $[W_2(OH)_4]^{2+}$ fragments are shown on Fig. 4c with a dotted line. Most interesting is a back donation from the filled $9b_2$ W–W π-based orbital to the unoccupied π_7 $6b_2$ COT^{2-} orbital, although the difference in energy between these two is approximately 5 eV.

The picture of bonding that emerges for $W_2(COT)(OH)_4$ is a smooth replacement of the donor orbitals of two OR^- groups by appropriate π MOs of the puckered COT^{2-} ligand. As Cayton *et al.* pointed out in their study of $W_2(COT)(NH_2)_4$, the puckered antifacial COT ligand serves essentially as a source of two allyl groups, one of which interacts with each W center.[8a] As expected, the W–W triple bond of $W_2(OR)_6$ is preserved in $W_2(COT)(OH)_4$, albeit with greater mixing of the W–W and ligand orbitals because of the lower symmetry.

The optimized DFT geometry for $W_2(COT)(OH)_4$ under C_{2v} symmetry is shown in Fig. 5. The calculated W–W bond length is 2.394 Å, which is close to the experimental W–W bond length of 2.389 Å in $W_2(COT)(O^tBu)_4$. In addition to the W–W bond length, the geometric structure of $W_2(COT)(OH)_4$ correlates closely with the experimental structural features of $W_2(COT)(NMe_2)_4$,[8a] $W_2(allyl)_2(NMe_2)_4$,[8b] and $W_2(COT)(O^tBu)_4$ (Table 4). The only exception is found for the N–W–N angles in the bis-allyl compound which are 120° instead of approximately 90°, as for the E–W–E bonds in the other complexes. The bulky and rigid COT ligands push the corresponding alkoxides or amides closer to each other more so than the relatively loose set of two allyl ligands.

The COT ring is predicted to adopt a puckered antifacial orientation, and the calculated W–W–O and O–W–O angles, 113 and 89°, respectively, are very close to the corresponding W–W–O and O–W–O angles in $W_2(COT)(O^tBu)_4$. The t-butoxide crystal structure exhibits two distinct W–W–O angles with averaged values of 115 and 108° along with two distinct O–W–O angles of 92 and 90°. This slight distortion of symmetry is most likely the result of a crystal packing effect since it is not observed in the solution NMR studies.

The predicted puckering of the COT ring in $W_2(COT)(OH)_4$ is consistent with the "bis-allyl" analogy advanced by Cayton *et al.*[8a] We find that the allylic C_3 fragments in $W_2(COT)(OH)_4$ form a dihedral angle of 40.0° with the plane formed by the vectors that connect the two C_3 fragments. Furthermore, the four symmetry equivalent C–C bond lengths within the allylic C_3 fragments (1.437 Å) are significantly shorter than the other four C–C bonds (1.475 Å), consistent with greater negative charge localization and therefore greater multiple bond character in the allylic ends of the COT ligand.

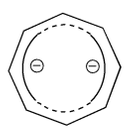

Table 3 Energies and compositions of selected MOs of $W_2(COT)(OH)_4$

MO	Energy/eV	Occupation	Major contributions W_2	COT
19b$_1$	−1.03	0	29% π*, 17% σ*, 12%δ*	
13a$_2$	−1.06	0	46% π*, 11% δ*	14% 4a$_2$
18b$_1$	−2.00	0	28% σ*, 27% π*	21% 6b$_2$
21a$_1$	−2.50	0	42% δ	14% 7a$_1$
17b$_1$	−2.70	0	49% δ*	14% 6b$_2$
20a$_1$	−4.65	2	29% π, 15% δ, 11% σ	19% 7a$_1$
14b$_2$	−5.64	2	33% π	21% 6b$_1$
12a$_2$	−5.70	2	7% δ*	60% 4a$_2$
19a$_1$	−6.49	2	41% σ, 26% π	
18a$_1$	−6.92	2	15% π	38% 7a$_1$

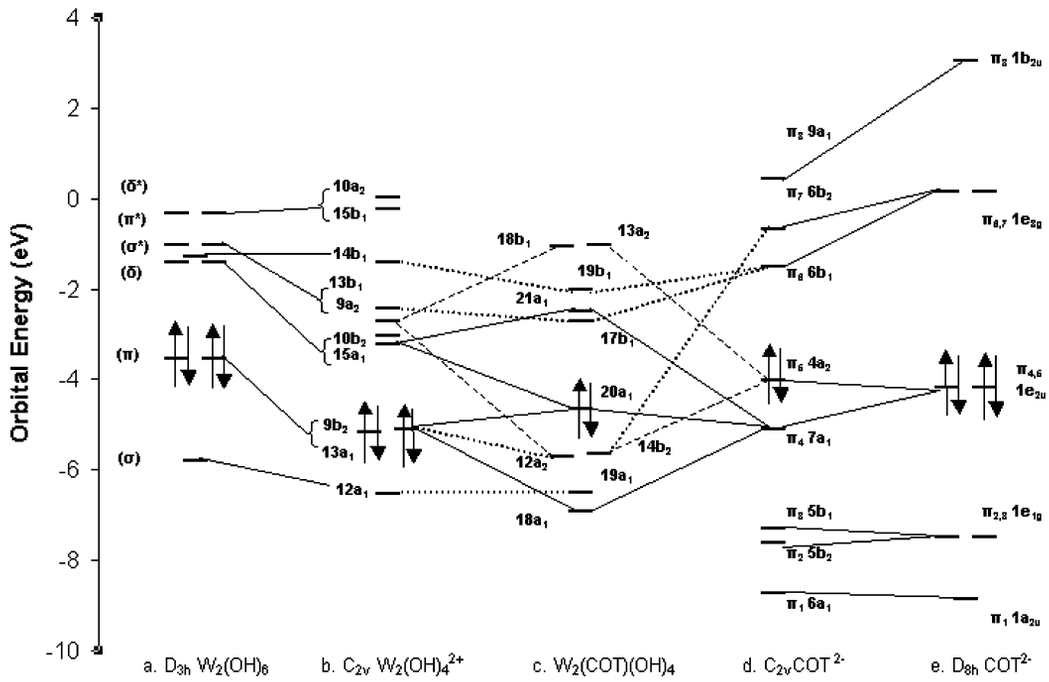

Fig. 4 From left to right: (a) Metal-based MOs of eclipsed $W_2(OH)_6$; (b) Metal-based MOs of $[W_2(OH)_4]^{2+}$, obtained by removing two OH^- ligands from eclipsed $W_2(OH)_6$; (c) Selected MOs of $W_2(COT)(OH)_4$; (d) π MOs of puckered COT^{2-} under C_{2v} symmetry; and (e) π MOs of planar COT^{2-}.

Fig. 5 Molecular drawings of the optimized geometry of $W_2(COT)(OH)_4$, viewed down three independent axes.

In order to evaluate the facile 1,2-allyl shift occurring on the NMR timescale, we performed two single-point calculations locking the COT ring into both the μ-η^5,η^5- and μ-η^4-η^4- bonding modes. The molecular geometry was optimized at both endpoints without symmetry constraints. It was found that the synfacial structure was 13.7 kcal mol^{-1} higher in calculated total bonding energy than the corresponding antifacial structure. Thus, at a minimum, there is a 13.7 kcal mol^{-1} rotational barrier associated with the 1,2-allyl shift in these compounds. We also undertook an intrinsic reaction coordinate search to map out any transition states lying between the two structures (Fig. 6). The search found a transition structure lying 20.2 kcal mol^{-1} higher in energy than the antifacial structure in which the line connecting the C_1–C_5 axis is skewed 9.5° from the W–W axis. Therefore, the barrier between antifacial and synfacial

Table 4 Experimental bond lengths (Å) and angles (°) for compounds $W_2(allyl)_2(NMe_2)_4$ (**I**), $W_2(COT)(NMe_2)_4$ (**II**), **1c**, and calculated parameters for model compound $W_2(COT)(OH)_4$ (**III**). E = N (**I**,**II**) or O (**1c**,**III**)

	I	II	1c	III
W–W	2.48	2.43	2.39	2.40
W–E	1.99	2.03	1.94	1.93
	1.97	1.96	1.93	
			1.92	
			1.91	
W–C1	2.44	2.45	2.45	2.46
		2.43	2.44	
			2.42	
			2.41	
W–C2	2.22	2.26	2.25	2.27
		2.26	2.25	
		2.24	2.24	
		2.23	2.23	
W–C3	none	2.32	2.32	2.33
		2.32	2.32	
W–W–E	115.6	115.3	115.8	113.3
	112.2	114.8	115.5	
		109.9	108.7	
		109.3	107.2	
E–W–E	120.5	89.9	92.3	89.0
	120.0	90.7	90.2	

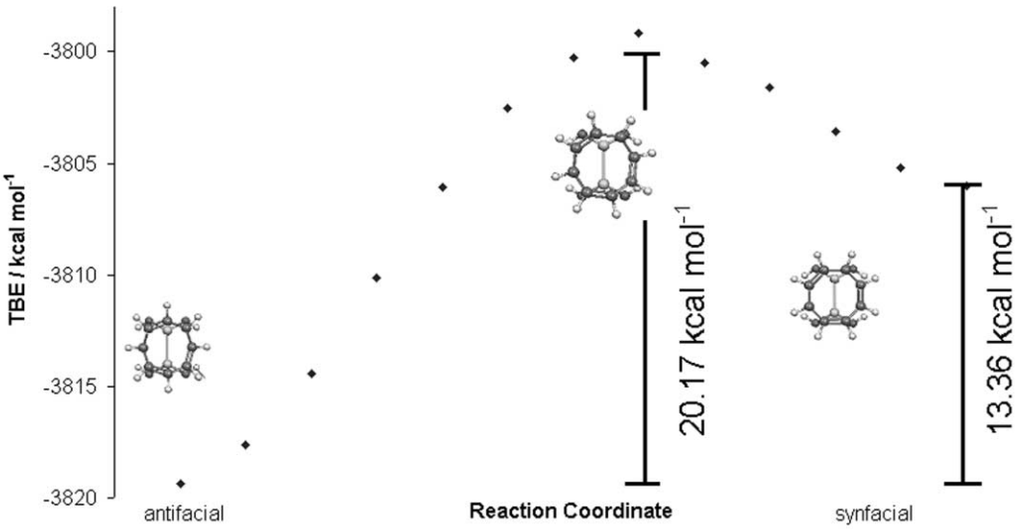

Fig. 6 Intrinsic reaction coordinate search, Rotating COT ring in $W_2COT(OH)_4$ by increments of 4°.

structures in alkoxides $W_2COT(OR)_4$ should correspond to approximately 20.2 kcal mol^{-1}, and as expected the most stable antifacial structure is the lone structure seen in the limiting low temperature regime.

As mentioned previously, compound **1c**, its amide precursor **II**, and the analogous amido bis-allyl compound **I**, show obvious similarities in their bonding parameters (Table 4). Notably, the W–W bond length differs by less than 0.1 Å in the series. Similarly, the W–C distances show that the bis-allyl and COT ligands are interacting with the dimetal unit in a similar fashion in all three instances. This would imply that there might be a similar rotational barrier for the COT ligand in **II** and although the COT ring was found to be fluxional in **II**, the exact mechanism of exchange (1–2 shift *versus* 1–3 shift) was not established.[8]

Finally, we can use the calculated MO energies to comment on the observed electronic transitions seen in the electronic absorption spectra of the $W_2(COT)(OR)_4$ complexes. The HOMO–LUMO separation in $W_2(COT)(OH)_4$ is 1.95 eV, which corresponds to $\lambda = 640$ nm. This value is satisfyingly close to the observed experimental absorption maximum in the $W_2(COT)(OR)_4$ complexes, which is typically at about 580 nm. This transition is predicted to occur from one of the predominantly W–W π MOs ($20a_1$) to an MO ($17b_2$) that is W–COT and W–OH antibonding. We are pleased that these initial DFT calculations on a large system with low symmetry as found for $W_2(COT)(OH)_4$ seem to be giving results in excellent accord with the available experimental data.

Concluding remarks

Although COT seems to be unreactive towards reduction by ditungsten alkoxides, it is evident that the $W_2(COT)(NMe_2)_4$ compound provides a reactive precursor to ditungsten compounds supported by both alkoxides and COT. The 1,2-shift that is active in these compounds proves to be similar to the related dinuclear COT compounds first explored by Cotton and coworkers.[3–6]

It is reasonable to suspect that the COT-bridged ditungsten tetraalkoxides will mimic some of the rich reactivity of other ditungsten alkoxides. This is already apparent in the facile alcohol exchange seen in the reaction of $W_2COT(O^tBu)_4$ with neopentyl alcohol; similar reactions have been noted for other ditungsten alkoxides.[9] The calculations on $W_2(COT)(OH)_4$ show that there is considerable metal to COT electron donation. One can envision the COT approaching COT^{4-}, leading to more of a $(W{=}W)^{8+}$ center. This would be similar to the MM bond found in $W_2(OR)_8$.[12a,b] The $W_2(OR)_8$ compounds show interesting coordination activation of unsaturated organics such as alkenes, alkynes, allenes, and ketones. It is anticipated that studies directed toward the activation of such groups with $W_2(COT)(OR)_4$ may also lead to similar results.

Experimental

Instrumentation

All NMR spectra were obtained on either a Bruker DRX-500 or DPX-400 spectrophotometer. ^{13}C NMR spectra were recorded at 100 MHz. ^1H NMR spectra were referenced to the residual proteo impurities in toluene-d_8 ($Ar–CD_2H$ at 2.09 ppm). ^{13}C NMR spectra were referenced to toluene-d_8 ($Ar–^{13}CH_3$ at 20.4 ppm). Toluene-d_8 was dried over K(s) and stored over 4 Å molecular sieves. EI mass spectra were obtained on a double-focusing, magnetic sector Kratos MS-890 instrument using either perfluorokerosene or 2,4,6-trisperfluorononyl-1,3,5-triazine as the calibrant. HRMS was obtained first in high-performance nominal mass mode and after acquisition was converted to accurate mass by comparison to a triazine lock mass. Electrospray TOF MS was obtained on a Micromass Q TOF-II instrument using solutions in dry THF. Visible spectra were obtained in cuvettes fitted with J-Young valves on a Perkin-Elmer Lambda 900 spectrometer. Elemental analyses were performed by Atlantic Microlabs (Atlanta, GA).

Methods and reagents

All manipulations were performed on a standard Schlenk line or in a dry box under an atmosphere of 99.9% argon or 99.99% N_2. Molecular sieves (4 Å, Linde) were dried overnight under dynamic vacuum (10 mTorr, 300 °C) before use.

$W_2(COT)(NMe_2)_4$ was synthesized as previously reported with the exception of substituting K_2COT for $Li_2COT{\cdot}(THF)_x$.[8a] 1,3,5,7-cyclooctatetraene (Aldrich, 97%) was stored in the dark at −35 °C and vacuum transferred when needed. K_2COT was made by carefully stirring excess COT with two equivalents of K(s) in THF for one day under a positive pressure of argon, after which the volatile components were removed to give a purple powder in quantitative yields. **Caution!** Dry K_2COT reacts explosively with air. Toluene and pentane were dried over Na and Na/K alloy, respectively, and stored over molecular sieves. Neopentanol was triply sublimed before use (80 mTorr, 25 °C) and t-butanol was stored at 30 °C over molecular sieves. Isopropanol and ethanol were dried by stirring over CaH_2 for 24 h prior to use.

Syntheses

Cyclooctatetraenyltetrakis(neopentoxy)ditungsten (1a). To a stirred mixture of $W_2(COT)(NMe_2)_4$ (0.500 g, 0.771 mmol) and n-pentane (50 mL) was added neopentanol (0.270 g, 3.09 mmol) in one portion. The color of the solution immediately changed from forest green to purple. The mixture was stirred at ambient temperature for 1 h after which the volatile components were removed under reduced pressure. The solid was dried under vacuum (80 mTorr, 50 °C, 1 day) to yield a fine, dark purple powder (0.470 g, 75%). An identical reaction employing eight equivalents of neopentanol yielded the same product after subliming out the excess neopentanol.

Alternatively, **1a**, was made by adding **1c** (0.250 g, 0.33 mmol) to a solution of neopentyl alcohol (0.1211 g, 1.37 mmol, 4.2 equiv) in 10 mL of pentane, allowing the mixture to stir for 12 h, and removing the volatiles under reduced pressure to give **1a** (0.256 g, 94.6%). ^{1}H NMR data (toluene-d_8, 400 MHz, δ): 27 °C, 1.06 (s, 36 H, CH_3), 3.98 (broad, 2H, H_a–H_b), 4.02 (d, $^1J_{HH}$ = 10 Hz, 4H, CH_2), 4.50 (d, $^1J_{HH}$ = 10 Hz, 4H, CH_2), 5.34 (broad, 4H, H_c), 5.66 (broad, 2H, H_a–H_b); −80 °C, 1.22 (s, CH_3, 36H), 3.62 (t, $^3J_{Ha,b–Hc}$= 9.6 Hz, 2H, H_a–H_b), 4.06 (d, $^1J_{HH}$ = 8.8 Hz, 4H, CH_2), 4.70 (d, $^1J_{HH}$ = 8.8 Hz, 4H, CH_2), 5.22 (overlapping dd, $J_{Hc–Ha,b}$= 8.4 Hz, 4H, H_c), 5.46 (t, $^3J_{Ha,b–Hc}$= 7.2 Hz, 2H, H_a–H_b). Identification of ^{1}H NMR signals arising from bound COT is made according to the preceding, labelled diagram (Results and discussion), where it is not possible to uniquely identify H_a and H_b.

EXSY ^{1}H NMR showed chemical exchange cross peaks between the cyclooctatetraenyl protons H_a, H_b, and H_c at 27 °C, while the exchange between H_a and H_b ceased below – 40 °C. ^{13}C NMR data (toluene-d_8, 100 MHz, 27 °C, δ): 25.7 (CH_3), 32.9 (CMe_3), 51.4 (COT), 81.2 (CH_2), 97.7 (COT), 101.3 (COT). ^{13}C NMR spectral assignments were confirmed by DEPT. UV-Vis data (toluene): λ_{max} = 583 nm (ε = 1790 M^{-1} cm^{-1}). Nominal MS for $W_2O_4C_{28}H_{52}$: 820.2 (M^+), 749.1 (M–C_5H_{11}•)$^+$, 393.1, 57.1 ($C_4H_9^+$). HRMS calc. for $W_2O_4C_{28}H_{52}$: 820.2913. Found 820.2891.

Cyclooctatetraenyltetrakis(isopropoxy)ditungsten (1b). A vacuum transfer flask was filled with $W_2(COT)(NMe_2)_4$ (0.400 g, 0.614 mmol), n-pentane (50 mL), and a magnetic stir bar. The contents were frozen at −78 °C under a nitrogen atmosphere, and the resultant solid mixture was immediately placed under vacuum. Excess isopropanol (10 mL) was condensed from CaH_2 onto the solid *via* vacuum transfer, and the mixture was allowed to slowly warm to room temperature with stirring. As the mixture warmed, the color of the solution changed color from green to burgundy to purple. The mixture was stirred at ambient temperature for 1 h after which the volatile components were removed under reduced pressure. The purple solid was dried under vacuum (80 mTorr, 50 °C, 1 day) to yield a fine purple powder (0.505 g, 92%). ^{1}H NMR data (toluene-d_8, 400 MHz, δ): 27 °C, 1.29 (d, $^3J_{HH}$ = 6.0 Hz, 12 H, CH_3), 1.35 (d, $^3J_{HH}$ = 6.0 Hz, 12H, CH_3), 4.03 (broad, 2H, H_a–H_b), 5.29 (sept, $^3J_{HH}$ = 6.0 Hz, 4H, CH), 5.35 (broad, 4H, H_c), 5.64 (broad, 2H, H_a–H_b); −60 °C, 1.41 (d, $^3J_{HH}$ = 7.5 Hz, 12 H, CH_3), 1.47 (d, $^3J_{HH}$ = 6 Hz, 12H, CH_3), 3.84 (t, $^3J_{HH}$ = 10 Hz, 2H, H_a–H_b), 5.30 (overlapping dd,$^3J_{HH}$ = 10 Hz, H_c, 4H), 5.45 (sept, $^3J_{HH}$ = 6.0 Hz, 4H, CH), 5.64 (t, $^3J_{HH}$ = 7.5 Hz, H_a–H_b, 2H) ^{13}C NMR (toluene-d_8, 100 MHz, 27 °C, δ): 25.3 (CH_3), 27.5 (CH_3), 52.4 (COT), 70.8 (CH), 97.0 (COT), 101.1 (COT). ^{13}C NMR spectral assignments were confirmed by DEPT. UV-Vis data (toluene): λ_{max} = 573 nm (ε = 1822 M^{-1} cm^{-1}). MS for $W_2O_4C_{20}H_{36}$: 708.3 (M^+), 667.3 (M–isoprene•)$^+$, 563.1 (M–isoprene–COT)$^+$, 521.1 (M–2isoprene•–COT)$^+$, 104.1 (COT^+). EA calc. for $W_2O_4C_{20}H_{36}$: C, 33.92%; H, 5.12%. Found: C, 33.20%; H, 5.73%.

Cyclooctatetraenyltetrakis(tert-butoxy)ditungsten (1c). To a stirred mixture of $W_2(COT)(NMe_2)_4$ (0.500 g, 0.771 mmol) and n-pentane (50 mL) was added a solution of t-butanol (0.240 g, 3.39 mmol) in 25 mL of pentane. The alcoholic solution was added in one portion over the course of several minutes. The color of the solution immediately changed from forest green to burgundy to purple. The mixture was stirred at ambient temperature for 1 h after which the volatile components were removed under reduced pressure. Pentane was added to the solid and the soluble portion transferred and dried under vacuum (80 mTorr, 30 °C, 30 min) to yield a clumpy, dark indigo powder (0.43 g, 73%). It is not recommended to dry this product under vacuum at temperatures in excess of *ca.* 50 °C as it seems that thermal decomposition occurs above these temperatures accompanied by a color change from indigo to green. Identical reactions employing greater than four equivalents of t-butanol lead to the same product. Suitable crystals for X-ray diffraction were obtained by slowly evaporating a toluene solution in the dry box to give dark purple needles. ^{1}H NMR data (toluene-d_8, 400 MHz, δ): 27 °C, 1.45 (broad s, 36 H, CH_3), 3.8–4.4 (very broad s, 2H, COT), 5.0–6.0 (very broad s, 6H, COT); −30 °C, 1.56 (s, CH_3, 36H), 3.97 (t, $^3J_{Ha,b–Hc}$ = 10.3 Hz, 2H, H_a–H_b), 5.26 (overlapping dd, $^3J_{Hc–Ha,b}$ = 9.8 Hz, 4H, H_c), 5.77 (t, $^3J_{Ha,b–Hc}$ = 8.2 Hz, 2H, H_a–H_b). ^{13}C NMR data (toluene-d_8, 100 MHz, 27 °C, δ): 32.3 (CH_3), 78.1 (CMe_3), 54.0 (COT), 96.0 (COT). UV-Vis data (toluene): λ_{max} = 580 nm (ε = 1694 M^{-1} cm^{-1}). Nominal MS for $W_2O_4C_{24}H_{44}$: 764.2 (M^+), 520.9 (M–WC_4H_{10})$^+$, 59.0 (Me_2COH)$^+$. HRMS calc. for $W_2O_4C_{24}H_{44}$: 764.2276. Found 764.2319.

Reactions of COT with various ditungsten alkoxides

A tenfold excess of COT (0.15 g, 0.14 mmol) was vacuum transferred onto a frozen solution of the ditungsten alkoxide (0.015 g, 0.014 mmol for $W_2(OCH_2{}^tBu)_6(py)_2$; 0.011 g, 0.014 mmol for $W_2(O^tBu)_6$; 0.015 g, 0.014 mmol for $W_2(OCH_2{}^tBu)_8$) dissolved in 50 mL toluene. The solutions were allowed to warm to room temperature over the course of approximately 1 h and were stirred at room temperature for 12 h. After stirring, the volatile components were removed under reduced pressure to yield solid products. ^{1}H NMR analysis of the reaction products revealed that in each case no reaction had occurred and the starting ditungsten alkoxide along with unreacted COT was recovered. In the case of $W_2(OCH_2{}^tBu)_6(py)_2$, heating the reaction to 80 °C while stirring for 2 h did not lead to a reaction and again, the starting alkoxide was recovered after removal of the volatile components.

Reaction of $W_2(OCH_2{}^tBu)_6(py)_2$ and COT in presence of excess ethanol

COT (0.15 g, 0.14 mmol) and $W_2(OCH_2{}^tBu)_6(py)_2$ (0.015 g, 0.014 mmol) were mixed in a vacuum transfer flask with approximately 20 mL toluene, frozen, and then evacuated. Excess ethanol (10 mL) was vacuum transferred onto the solution at −78 °C. As the mixture was allowed to warm, the solution slowly changed color from dark red to navy blue. The mixture was allowed to warm to room temperature over the course of 1 h and was stirred for 2 h at room temperature. The volatile components were then removed under reduced pressure to yield a blue solid. Electrospray TOF MS analysis showed the product mixture consisted of a higher molecular weight compound with the highest weight fragment at m/z = 1888.

Computational procedures

Density functional theory calculations were performed using the Amsterdam Density Functional (ADF) program, version 2000.01, developed by Baerends *et al.*[13] and vectorized by Ravenek.[14] The numerical integration scheme used was developed by te Velde *et al.*,[15] and the geometry optimization procedure was based on the method of Versluis and Ziegler.[16] Geometry optimizations were carried out under full C_{2v}

symmetry using the local exchange-correlation potential of Vosko *et al.*[17] and the non-local exchange and correlation corrections of Perdew and Wang (PW91).[18] For W, the electronic configuration was described using a double-ζ STO basis for 5s and a triple-ζ for 6s, 5p, 5d, and 4f, augmented by a 6p and a 5f polarization function. The core was frozen and was defined to be 4d and below. For oxygen and carbon, a triple-ζ STO basis was used for the valence 2s and 2p orbitals, augmented by a 3d and a 4f polarization function, with the core 1s orbital frozen. Hydrogen was also treated using a triple-ζ STO basis for its 1s orbital, and was augmented with a 2p and a 3d polarization function. All atoms were also corrected for relativistic effects using the zeroth order regular approximation (ZORA) method.[19] All accuracy and convergence parameters were left at the default level, with the exception of the general integration accuracy, which was set to 6.0.

Crystal structure analysis

Crystal data and experimental conditions for the t-butoxide are listed in Table 1. The molecular structure is illustrated in Figs. 2 and 3 and atoms are drawn with 50% probability displacement ellipsoids. Selected bond lengths and angles with standard deviations in parentheses are presented in Table 2. The data collection crystal was a dark purple, rectangular block. Examination of the diffraction pattern on a Nonius Kappa CCD diffractometer indicated a monoclinic crystal system. All work was done at 150 K using an Oxford Cryosystems Cryostream cooler. The data collection strategy was set up to measure a quadrant of reciprocal space with a redundancy factor of 5.0, which means that 90% of the reflections were measured at least 5 times. A combination of ϕ and ω scans with a frame width of 1.0° was used. Data integration was done with Denzo.[20] Scaling and merging of the data was done with Scalepack;[20] application of an absorption correction is inherent in this treatment and is reflected in the scale factor range of 7.64–11.27. Merging the data and averaging the symmetry equivalent reflections resulted in an R_{int} value of 0.035.

The maXus[21] package indicated the space group to be $P2_1/c$ based on the systematic absences. The positions of the two W atoms were located by the Patterson method in SHELXS-86.[22] The rest of the molecule was found by standard Fourier methods.

Full-matrix least-squares refinements based on F^2 were performed in SHELXL-93.[23] The methyl group hydrogen atoms were added at calculated positions using a riding model with $U(H) = 1.5 * U_{eq}$ (bonded C atom). For each methyl group, the torsion angle which defines its orientation about the C–C bond was refined. All of the eight hydrogen atoms of the COT ligand were located on a difference map and initially were added to the model as fixed contributions. These eight hydrogen atoms were subsequently refined isotropically. An extinction parameter was also introduced in the final cycles of refinement. Neutral atom scattering factors were used and include terms for anomalous dispersion.[24]

Full crystallographic details (atomic coordinates, thermal parameters, bond lengths, and bond angles) for **1c** have been deposited in the Cambridge Crystallographic Database. See Instructions for Authors, *J. Chem. Soc., Dalton Trans.*, 2002, Issue 1. Any request to the CCDC for this material should quote the full literature citation and the CCDC reference number 186395. However, the following weblink may be more convenient.

See http://www.rsc.org/suppdata/dt/b2/b205130n/ for crystallographic data in CIF or other electronic format.

Acknowledgements

We wish to thank Mr. Johnie Brown and the Ohio State Campus Chemical Instrumentation Center for help with TOFMS and EIMS experiments. We also wish to thank Mr. Karl Vermillion for help with the low-temperature EXSY experiments. CBH and MLD thank OSU for teaching assistantships. We wish to express thanks to the Ohio Supercomputing Center for a grant of calculational time.

References

1 (*a*) M. H. Chisholm, *J. Chem. Soc., Dalton Trans.*, 1996, 1789; (*b*) J. T. Barry, S. T. Chacon, M. H. Chisholm, J. C. Huffman and W. E. Streib, *J. Am. Chem. Soc.*, 1995, **117**, 1974.
2 J. T. Barry, J. C. Bollinger, M. H. Chisholm, K. C. Glasgow, J. C. Huffman, E. A. Lucas, E. B. Lubkovsky and W. E. Streib, *Organometallics*, 1999, **18**, 2300.
3 F. A. Cotton and M. D. La Prade, *J. Am. Chem. Soc.*, 1968, **90**, 2026.
4 F. A. Cotton and W. T. Edwards, *J. Am. Chem. Soc.*, 1968, **90**, 5412.
5 F. A. Cotton and S. A. Koch, *J. Am. Chem. Soc.*, 1977, **99**, 7371.
6 F. A. Cotton, S. A. Koch, A. J. Schultz and J. M. Williams, *Inorg. Chem.*, 1978, **17**, 2093.
7 (*a*) R. B. King, *Organomet. Synth.*, 1965, 126; (*b*) M. D. Rausch and G. N. Schrauzer, *Chem. Ind.*, 1959, 957; (*c*) T. A. Manuel and F. G. A. Stone, *J. Am. Chem. Soc.*, 1960, **82**, 366; (*d*) Uwe Richter, Juergen Heck and Joachim Reinhold, *Inorg. Chem.*, 1999, **38**, 77; (*e*) Uwe Richter, Juergen Heck and Joachim Reinhold, *Inorg. Chem.*, 2000, **39**, 658.
8 (*a*) R. H. Cayton, S. T. Chacon, M. H. Chisholm, K. Folting and K. G. Moodley, *Organometallics*, 1996, **15**, 992; (*b*) M. H. Chisholm, M. J. Hampden-Smith and J. C. Huffman, *J. Am. Chem. Soc.*, 1988, **110**, 4070.
9 M. H. Chisholm, *Acc. Chem. Res.*, 1990, **23**, 419 and references therein.
10 J. Li and B. E. Bursten, in *Computational Organometallic Chemistry*, ed. T. R. Cundari, Marcel Dekker, New York, 2001, p. 315.
11 B. E. Bursten and W. F. Schneider, in *Metal–Metal Bonds and Clusters in Chemistry and Catalysis*, ed. J. P. Fackler, Plenum Press, New York, 1990, p. 19.
12 (*a*) T. A. Budzichowski, M. H. Chisholm, K. Folting, J. C. Huffman and W. E. Streib, *J. Am. Chem. Soc.*, 1995, **117**, 7428; (*b*) J. C. Bollinger, M. H. Chisholm, D. R. Click, K. Folting, C. M. Hadad, D. B. Tiedtke and P. J. Wilson, *J. Chem. Soc., Dalton Trans.*, 2001, **14**, 2074.
13 (*a*) E. J. Baerends, D. E. Ellis and P. Ros, *Chem. Phys.*, 1973, **2**, 41; (*b*) E. J. Baerends and P. Ros, *Chem. Phys.*, 1973, **2**, 52; (*c*) G. te Velde and E. J. Bearends, *J. Comput. Phys.*, 1992, **99**, 84; (*d*) C. G. Fonseca, O. Visser, J. G. Snijders, G. te Velde and E. J. Baerends, in *Methods and Techniques in Computational Chemistry*, METECC-95, ed. E. Clementi and G. Corongiu, STEF, Cagliara, Italy, 1995, p. 305.
14 W. Ravenek, in *Algorithms and Applications on Vector and Parallel Computers*, ed. H. J. J. te Riele, T. J. Dekker and H. A. van de Horst, Elsevier, Amsterdam, 1987.
15 P. M. Boerrigter, G. te Velde and E. J Baerends, *Int. J. Quantum Chem.*, 1998, 87.
16 L. Versluis and T. Ziegler, *J. Chem. Phys.*, 1988, **88**, 322.
17 S. H. Vosko, L. Wilk and M. Nusair, *Can. J. Phys.*, 1980, **58**, 1200.
18 J. P. Perdew, *Phys. Rev. B.*, 1992, **46**, 6671.
19 E. van Lenthe, A. E. Ehlers and E. J. Baerends, *J. Chem. Phys.*, 1999, **110**, 8943.
20 Z. Otwinowski and W. Minor, DENZO, in *Methods in Enzymology*, vol. 276, *Macromolecular Crystallography, Part A*, ed. C. W. Carter, Jr and R. M. Sweet, Academic Press, New York, 1997, p. 307.
21 S. Mackay, W. Dong, C. Edwards, A. Henderson, C. Gilmore, N. Stewart, K. Shankland and A. Donald, *maXus*, the University of Glasgow, Glasgow, Scotland, 2000.
22 G. M. Sheldrick, SHELXS-86, *Acta Crystallogr., Sect. A*, 1990, **46**, 467.
23 G. M. Sheldrick, *SHELXL-93*, Universitat Göttingen, Germany, 1993.
24 *International Tables for Crystallography*, Kluwer Academic Publishers, Dordrecht, 1992, vol. **C**.